07

A magnetoelectric gyrator based on three-layer symmetric structures: theory and experiment

© D.A. Filippov,[1] T.A. Galkina,[1] I.N. Manicheva,[1] Jitao Zhang[2]

[1] Yaroslav-the-Wise Novgorod State University,
173003 Veliky Novgorod, Russia
[2] College of Electrical and Information Engineering, Zhengzhou University of Light Industry,
450002 Zhengzhou, China
e-mail: dmitry.filippov@novsu.ru

Received March 23, 2023
Revised July 7, 2023
Accepted July 9, 2023

The work is devoted theoretical and experimental studies of a magnetoelectric gyrator, consisting of an inductor coil, inside which there is a magnetoelectric heterostructure, which is a mechanically connected piezoelectric layer and two magnetic layers. Using the system of equations of elasto- and electrodynamics for the piezoelectric and magnetostrictive phases, expressions are obtained for the current/voltage conversion coefficient of the gyrator in terms of the phase parameters of the heterostructure. An experimental sample of a gyrator based on the Metglas/PZT/Metglas heterostructure was fabricated. Theoretically calculated and experimentally studied the frequency and load characteristics of the gyrator. It is shown that theoretical calculations are in good agreement with experimental data. Recommendations for the creation of gyrators with the highest current/voltage conversion efficiency are presented.

Keywords: gyrator, magnetostriction, piezoelectricity, magnetoelectric heterostructures, magnetoelectric effect.

DOI: 10.21883/0000000000

Introduction

The gyrator prototype as the fifth basic passive element of electronic circuits was first proposed by Tellegen in 1948 [1]. The gyrator can be realized using a circuit solution based on an operational amplifier [2]. The ideal gyrator, which acts as a capacitor-to-inductance coil converter, has proved to be very useful in the design of inductance coil filters; non-reciprocal current-voltage converters $(I-V)$ are widely used in radars with simultaneous receive-transmit functions, high-power wireless transmitters, etc. [3–5]. The proposed circuit solutions make the circuits rather bulky, requiring additional power supplies. However, the gyrator can be realized based on the magnetoelectric (ME) effect predicted in [6,7] and first experimentally detected in [8,9]. It is expedient to use magnetostriction piezoelectric heterostructures for realization of the ME gyrator, since the magnitude of the ME effect in them is several orders of magnitude larger than in single-crystals, which opens wide prospects for their use in electronics [10–12].

A classic ME gyrator consists of an inductance coil with a sample of ME material inside. The current-voltage conversion is performed as follows: an alternating current I_{in} is applied to the inductance coil, which creates an alternating magnetic field H in its internal area, in which the ME sample is located. Due to magnetostriction, this alternating magnetic field Hinduces strains in the magnetic component of the ME heterostructure, which are transmitted through the interface to the piezoelectric component, resulting in an electric voltage V_{out}. The $(I-V)$-conversion factor K_{IV}, equal to the ratio of the output voltage V_{out} to the input current value I_{in}, i.e. $K_{IV} = V_{out}/I_{in}$, depends both on the frequency of the variable input signal and on the geometrical parameters of the inductance coil, the parameters of the ME sample and the load resistance. Previously, the equivalent circuit method [13–16] was most commonly used in the study of ME gyrators. In this approach, the gyrator was typically represented as three interconnected domains: electrical domain (inductive port)-mechanical domain-electrical domain (capacitive port). The interaction between domains was carried out through electromechanical and magnetic mechanical coupling coefficients. The disadvantage of this method is that it is difficult to take into account the peculiarities of the ME heterostructure, for example, symmetric (three-layer) or asymmetric (two-layer), the influence of geometrical dimensions, material parameters. The aim of the present paper was to construct the theory of ME gyrator based on the general equations of elasto-dynamics and electrodynamics.

1. Theoretical model

As a model, let us consider a classical ME gyrator consisting of a coil, inside of which there is a symmetrical ME structure consisting of a piezoelectric plate with plates of magnetostriction material attached to both sides of the coil. The schematic representation of the gyrator and ME structure are shown in Figs. 1 and 2, respectively.

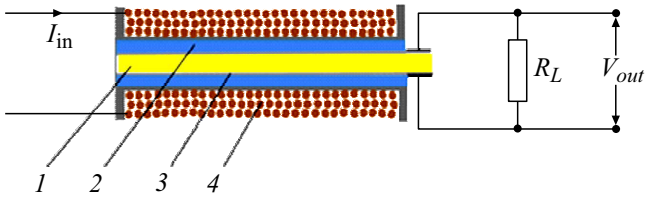

Figure 1. Schematic diagram of the gyrator: *1* — piezoelectric layer, *2* — magnetostriction layers, *3* — thin silver layer, *4* — inductance coil. Input current I_{in}, output voltage V_{out}, load resistance R_L.

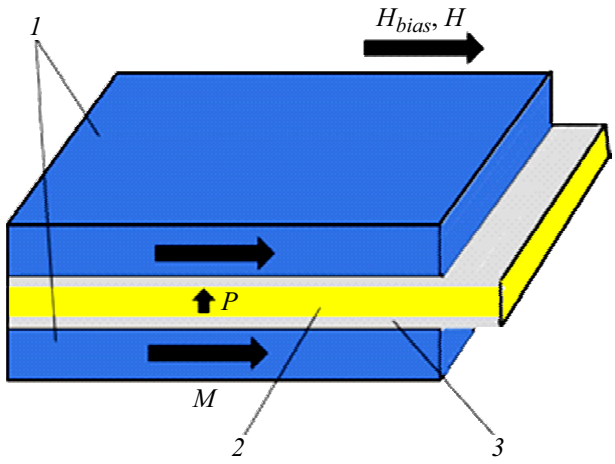

Figure 2. Schematic representation of the DOE structure: *1* — magnetostriction layer, *2* — piezoelectric layer, *3* — thin conductor (Ag) layer. The arrows show the directions of magnetization M, polarization P, sub-magnetization field H_{bias}, and alternating magnetic field H.

The choice of a symmetrical ME structure is due to the fact that when an asymmetrical magnetostriction-piezoelectric structure is placed in a magnetic field, longitudinal and bending oscillations can occur, weakening each other [17]. In symmetric structure, only longitudinal vibrations occur, resulting in more efficient ME interaction.

The initial equations underlying the model were the equations representing the generalized Hooke's law, as well as the equations of elasto-dynamics and electrodynamics, written in the following form:

$$S_1^p = \frac{1}{Y^p} T_1^p + d_{31}^p E_3^p, \tag{1}$$

$$S_1^m = \frac{1}{Y^m} T_1^m + q_{11}^m H_1^m, \tag{2}$$

$$D_3^p = \varepsilon_{33} E_3^p + d_{31}^p T_1^p. \tag{3}$$

Here S_1^p, S_1^m, T_1^p and T_1^m — components of strain and stress tensors for piezoelectric and magnetostriction phases, D_3^p — component of electric induction vector, E_3^p, H_1^m — components of electric and magnetic field strength vector in piezoelectric and magnetics, respectively, d_{31}^p, q_{11}^m — piezoelectric and piezo-magnetic moduli, $\varepsilon_{33} = \varepsilon_{33}^p \varepsilon_0$, ε_{33}^p — relative dielectric constant of piezoelectric, $\varepsilon_0 = 8.85 \cdot 10^{-12}$ F/m — dielectric constant, Y^p and Y^m — Young's moduli of piezoelectric and magnetostriction phases. By piezo-magnetic effect here we mean the effect of producing strains linear in magnitude of the alternating magnetic field H in the presence of a sub-magnetizing field H_{bias}, and the piezo-magnetic modulus q is defined as $q = \frac{\partial \lambda(H)}{\partial H}|_{H=H_{bias}}$, where $\lambda(H)$ — the magnetostriction of the magnetite.

Let us write down the equation of elasto-dynamics of the medium assuming that the displacements of piezoelectric and magnetostriction media are the same. Then, the equation of motion of the medium is written in the form

$$\bar{\rho} \frac{\partial^2 u_1}{\partial t^2} = \frac{\partial \bar{T}_1}{\partial x}. \tag{4}$$

Here $\bar{\rho} = \frac{\rho^m t^m + \rho^p t^p}{t^m + t^p}$ — mean value of sample density, $\bar{T} = \frac{T^m t^m + T^p t^p}{t^m + t^p}$ — mean value of stress tensor, $t^m = 2t^{m1}$ — thickness of two magnetostriction layers, t^{m1} — thickness of one magnetostriction layer, t^p — thickness of piezoelectric layer.

Expressing from equations (1) and (2) the components of the stress tensor through the components of the strain tensor and substituting them into equation (4), we obtain the equation for the displacement of the medium in the form of

$$\bar{\rho} \frac{\partial^2 u_1(x,t)}{\partial t^2} = \bar{Y} \frac{\partial^2 u_1(x,t)}{\partial x^2}, \tag{5}$$

where the designation $\bar{Y} = \frac{Y^m t^m + Y^p t^p}{t}$ — mean value of Young's modulus, $t = t^m + t^p$ — total thickness of the specimen is introduced.

Let us present the solution for the displacement in the form

$$u_1(x,t) = u_1(x) \exp(i\omega t), \tag{6}$$

Substituting this solution into equation (5) for the coordinate part, we obtain the equation

$$\frac{\partial^2 u_1(x)}{\partial x^2} + k^2 u_1(x) = 0, \tag{7}$$

where designation is introduced $k^2 = \frac{\bar{\rho}}{\bar{Y}} \omega^2$.

The solution of Eq. (7) is written as

$$u_1(x) = A \cos(kx) + B \sin(kx). \tag{8}$$

The integration constants A and B are determined from the condition of zero force on the left and right surfaces of the specimen, i.e.

$$t^m T^m(x = \pm L/2) + t^p T^p(x = \pm L/2) = 0. \tag{9}$$

Using these boundary conditions, we obtain the following expressions for the integration constants

$$A = 0, \quad B = \frac{t^m Y^m q_{11}^m H_1^m + t^p Y^p d_{31}^p E_3^p}{k \cos(\kappa)}, \tag{10}$$

where the dimensionless parameter is introduced $\kappa = \frac{kL}{2}$.

The electric current I_{out}, flowing in the output circuit can be found from the equation

$$I_{out} = \int_0^W dy \int_{-L/2}^{L/2} \frac{\partial D_3^p}{\partial t}\, dx. \qquad (11)$$

Substituting the solution (8) with consideration (10) into equation (3), and then the resulting expression into equation (11), and performing integration, we obtain

$$I_{out} = i\omega C t^p \left(\Delta_a E_3^p + \frac{Y^p d_{31}^p q_{11}^m}{\varepsilon_{33}} \frac{\tan(\kappa)}{\kappa} H_1^m \right). \qquad (12)$$

The notations are introduced here $C = \frac{\varepsilon_{33} WL}{t^p}$ — the capacitance of the piezoelectric plate, W — the width of the plate, $\Delta_a = 1 - k_p^2 + k_p^2 \frac{Y^p t^p}{Yt} \frac{\tan(\kappa)}{\kappa}$ — frequency-dependent parameter, $k_p^2 = \frac{Y^p (d_{31}^p)^2}{\varepsilon_{33}}$ — square of the electromechanical coupling coefficient.

Taking into account that, as it follows from Fig. 1, the output voltage $V_{out} = I_{out} R_L$, where R_L — load resistance, and the electric field strength $E_3^p = \frac{V_{out}}{t^p}$, after some simple transformations we obtain the following expression:

$$\frac{V_{out}}{\Delta_a} = i\omega\tau \left(V_{out} + \frac{Y^p d_{31}^p q_{11}^m t^p}{\varepsilon_{33}\Delta_a} \frac{\tan(\kappa)}{\kappa} H_1^m \right), \qquad (13)$$

where $\tau = R_L C$ — the recharge time RC of the chain.

The magnetic field strength H_1^m produced by a coil having $n = \frac{N}{L}$ turns per unit length is determined by the relation $H_1^m = I_{in} n$.

Introducing the coefficient $(I-V)$-transformation $K_{IV} = \frac{V_{out}}{I_{in}}$, we obtain the following expression for its modulus:

$$|K_{IV}| = \frac{Y^p d_{31}^p q_{11}^m}{\varepsilon_{33}\Delta_a} \left| \frac{\tan(\kappa)}{\kappa} \right| t^p n \frac{\omega\tau\Delta_a}{\sqrt{1 + (\omega\tau\Delta_a)^2}}. \qquad (14)$$

Let us introduce a capacitance $X_C = 1/\omega C$. Then, equation (14) can be rewritten as

$$|K_{IV}| = \frac{Y^p d_{31}^p q_{11}^m}{\varepsilon_{33}\Delta_a} \left| \frac{\tan(\kappa)}{\kappa} \right| t^p n \frac{(R_L/X_C)\Delta_a}{\sqrt{1 + ((R_L/X_C)\Delta_a)^2}}. \qquad (15)$$

Equations (14) and (15) allow us to calculate the modulus of the $(I-V)$-conversion coefficient as a function of frequency and load resistance using the material parameters and geometrical dimensions of the ME structure, as well as the characteristics of the inductance coil.

2. Experiment

For experimental studies, a gyrator consisting of a coil wound on a frame of size $20 \times 10 \times 5$ mm was fabricated. Inside the framework, there was a through rectangular hole of size 5.5×1.5 mm to accommodate the ME heterostructure. The frame was made by printing it on a 3D printer. A coil of copper wire with a diameter of $d = 0.35$ mm consisting of 152 turns was wound on the frame. The ME heterostructure consisted of a plate of PZT-19 piezoceramic with electrodes obtained by burning silver paste („Piezopribor“, Rostov-on-Don) and two layers of amorphous nanocrystalline alloy AMAG 212N produced by „Mstator PJS“ (Borovichi, Russia).

Values of material parameters

Parameter	Material	
	Piezoelectric PZT-19	Magnetic AMAG 212N
Plate length, mm	20	18
Plate width , mm	5	5
Layer thickness, mm	0.3	0.12
Density kg/m^3	7000	7700
Young's modulus, GPa	67	110
Relative dielectric permeability, ε_{33}^p	1750	–
Piezomodules: d_{31}^p, pC/N q_{11}^m, ppm/Oe	−175 –	– 0.3

The dimensions of the piezoelectric plate were $20 \times 5 \times 0.3$ mm, the dimensions of one layer of amorphous alloy — $18 \times 5 \times 0.06$ mm. The whole system was placed in a solenoid of diameter $D = 20$ mm and length $L = 180$ mm and containing $N = 500$ turns of 0.7 mm copper wire. A DC voltage from the UT 3010E power supply was applied to the solenoid to generate the submagnetizing field. An alternating voltage from the signal generator AKIP-3410/4 was applied to the gyrator coil. The load resistance was created using a resistance shop and its voltage was measured using an AKIP-2101 voltmeter and simultaneously monitored using an AKIP-4115/6A oscilloscope. During the measurements of frequency and load characteristics, the alternating current through the gyrator coil was in the range of 10−15 mA, which corresponded to the value of the alternating magnetic field strength of the order of 1 Oe. The non-resonant voltage value on the load resistance was a few tens of mV. The modulus of the $(I-V)$-conversion factor was calculated as the ratio of the voltage across the load resistance to the input current across the gyrator coil.

3. Results and discussions

Fig. 3 shows the frequency dependence of the modulus of the $(I-V)$-transformation coefficient calculated theoretically using equation (14) and obtained experimentally. The structure parameters presented in the table were used in the calculations.

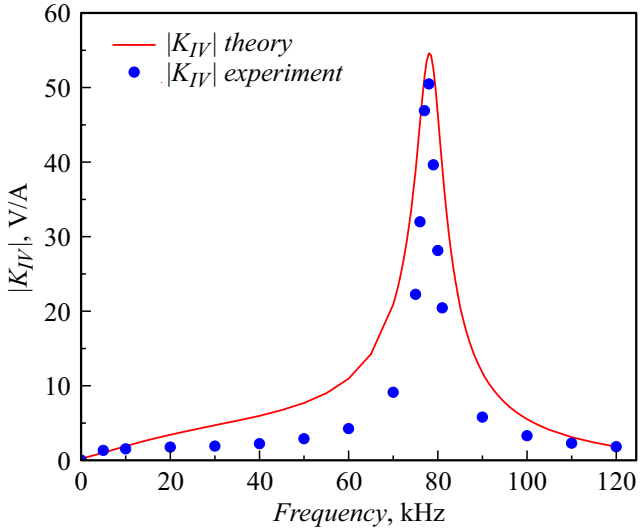

Figure 3. Frequency dependence of the modulus of the $(I-V)$-transformation coefficient. Solid line — theory, dots — experiment

.

As can be seen from Fig. 3, the frequency dependence of the modulus of the $(I-V)$-transformation coefficient has a resonant character. The fundamental resonant frequency corresponds to the condition where the dimensionless parameter κ is approximately equal to $\frac{\pi}{2}$. Hence for the resonant frequency we obtain the relation $f_{res} \cong \frac{1}{2L}\sqrt{\frac{Y}{\rho}}$.

As follows from equations (14) and (15), the magnitude of the coefficient depends on both the efficiency of the ME conversion and the design of the coil (magnetic field source), as well as the load resistance.

Outside the resonance area at small load resistances, when the ratio $\frac{R_L}{X_C} \ll 1$, equations (14) and (15) are simplified and take the form of

$$|K_{IV}| = \frac{Y^p d_{31}^p q_{11}^m}{\varepsilon_{33}} \left|\frac{\tan(\kappa)}{\kappa}\right| t^p n \omega \tau, \qquad (16)$$

$$|K_{IV}| = \frac{Y^p d_{31}^p q_{11}^m}{\varepsilon_{33}} \left|\frac{\tan(\kappa)}{\kappa}\right| t^p n (R_L/X_C). \qquad (17)$$

These equations show that in the low frequency area of the spectrum, when the dimensionless parameter $\kappa \ll 1$, the value $|K_{IV}|$ depends linearly on frequency and increases linearly with increasing load resistance. At large load resistances, when $\omega\tau \gg 1$, or, what is the same, $(R_L/X_C) \gg 1$, the magnitude of $|K_{IV}|$ reaches saturation, whose modulus of magnitude is

$$\lim_{(R_L/X_C)\to\infty} |K_{IV}| = |\alpha_E| t^p n, \qquad (18)$$

where α_E — ME coefficient on voltage, equal to

$$\alpha_E = \frac{Y^p d_{31}^p q_{11}^m}{\varepsilon_{33}\Delta_a} \frac{\tan(\kappa)}{\kappa}. \qquad (19)$$

Fig. 4 shows the load characteristic of the $(I-V)$-conversion coefficient module. In complete agreement with theory, at low load resistances, the value of $|K_{IV}|$ increases linearly with increasing load resistance and reaches saturation at high resistances, the higher the frequency, the earlier the saturation occurs.

It should also be noted that at saturation, the magnitude of $|K_{IV}|$, as well as the magnitude of the ME voltage coefficient α_E, is proportional to the ratio $\frac{d_{31}^p}{\varepsilon_{33}}$, while in the area, where $\frac{R_L}{X_C} \ll 1$, its magnitude is proportional to just d_{31}^p. It follows that materials such as gallium arsenide and quartz, which have ratios $\frac{d}{\varepsilon}$ of 0.024 and 0.05 m^2/C, respectively, versus 0. 011 m^2/C in lead zirconate titanate (PZT) and exhibiting good ME [18–21] characteristics, it is not appropriate to use them for gyrators in the low-frequency area because saturation K_{IV} is achieved only at high load resistances, but they show better performance than PZT-based gyrators in the high-frequency area. As an example, Fig. 5 shows the calculated load characteristics for gyrators at a frequency of 50 kHz, made on the basis of three-layer symmetrical heterostructures, where the amorphous alloy AMAG 212N is chosen as the magnetostriction phase, and the PZT gallium arsenide GaAs and quartz Q are chosen as the piezoelectric — PZT.

As can be seen from Fig. 5, for the CTC-based gyrator, the value of the $(I-V)$-conversion coefficient for a given gyrator design at a frequency of 50 kHz occurs at a load resistance value of a few kΩ, while for the GaAS-based gyrator, the value $|K_{IV}|$ begins to tend to saturation at a load resistance greater than 100 kΩ. At small load resistances, the value of $|K_{IV}|$ for the PZT-based gyrator exceeds that of the GaAs-based and Q-based gyrators, but at load resistances larger than 40 kΩ, the gyrators where GaAs and Q are used as piezo-electrics show better performance.

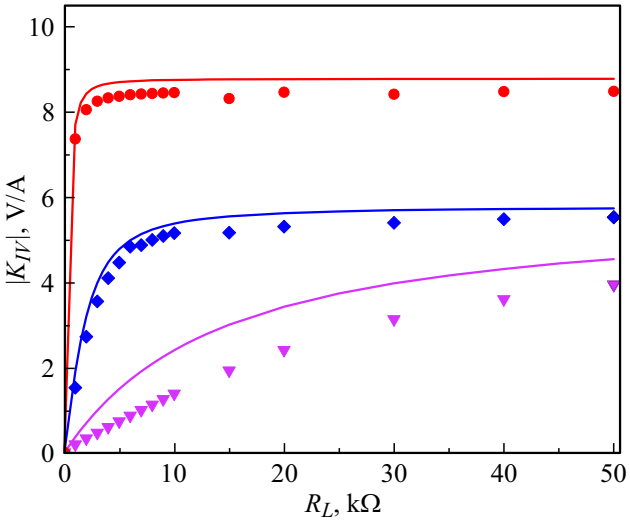

Figure 4. Load characteristic of the ME gyrator. Solid lines — theory, dots — experiment. –, ▼ — frequency $f = 1$ kHz; –, ♦ — $f = 10$ kHz; –, • — $f = 50$ kHz.

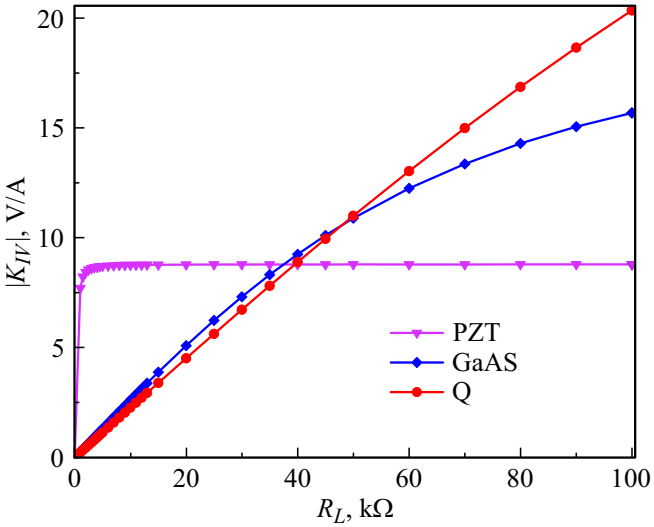

Figure 5. Load curves for symmetrical heterogeneous structures with different type of piezoelectric at 50 kHz.

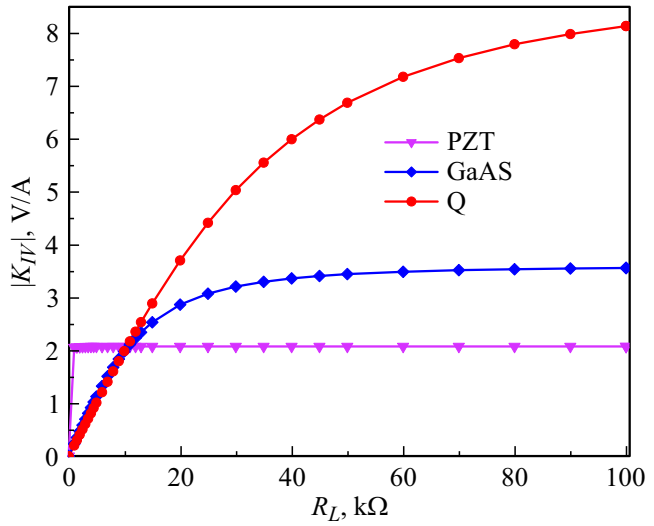

Figure 6. Load curves for symmetrical heterogeneous structures with different type of piezoelectric at 250 kHz.

It should also be noted that, as follows from equations (18) and (19), the magnitude of the coefficient $(I-V)$-transformation outside the resonance area decreases with increasing frequency due to an increase in the dimensionless parameter κ, standing in the denominator of equation (19). Fig. 6 shows the calculated transfer load characteristics for the same gyrators at a frequency of 250 kHz.

From the comparison of Figs. 5 and 6, it follows that in the low-frequency area of the spectrum at low load resistances, the PZT-based gyrator has better transmission characteristics than the gallium arsenide and quartz-based gyrators, while in the high-frequency area of the spectrum, the gallium arsenide and quartz-based gyrators show better characteristics compared to PZT.

Conclusion

The $(I-V)$-conversion factor K_{IV} depends on both the frequency of the AC input signal and the geometrical parameters of the inductance coil, ME sample parameters, and load resistance. At low load resistances, the value of $|K_{IV}|$ increases linearly with increasing load resistance and reaches saturation at high resistances, the higher the frequency, the earlier the saturation occurs. At saturation, the value of the $(I-V)$-conversion coefficient, as well as the value of the ME coefficient on voltage, is proportional to the ratio of the piezoelectric modulus to the dielectric permittivity, while in the low-frequency area at low load resistances its value is proportional simply to the value of the piezoelectric modulus. It follows that such materials as gallium arsenide and quartz, having a value of the ratio of piezoelectric modulus to dielectric permittivity greater than that of PZT, and demonstrating good ME characteristics, for the creation of gyrators in the low-frequency area to use inexpedient, because saturation of the coefficient $(I-V)$-conversion at them is achieved only at high load resistances, but in the high-frequency area they show better characteristics than gyrators based on PZT.

Funding

This study was supported by grant of the Russian Science Foundation, project № 22-19-00763, https://rscf.ru/project/22-19-00763/.

Conflict of interest

The authors declare that they have no conflict of interest.

References

[1] B.D.H. Tellegen. Philips Res., **3**, 81 (1948).
[2] I. Tatai, I. Zaharie. Rev. Sci. Instrum., **83** (11), 114702 (2012). DOI: 10.1063/1.4766332
[3] S. Bosco, F. Haupt, D.P. DiVincenzo. Phys. Rev. Appl., **7**, 2 (2017). DOI: 10.1103/ PhysRevApplied.7.024030
[4] S. Singer. IEEE Trans. Ind. Electron., **34** (3), 313 (1984). DOI: 10.1109/TIE.1987.350962
[5] A. Cervera, M. Evzelman, M.M. Peretz, S. Ben-Yaakov. IEEE Trans. Power. Electron., **30** (3), 1373 (2015). DOI: 10.1109/TPEL.2014.2317758
[6] L.D. Landau, E.M. Lifshitz *Electrodynamics of Continuous Media* (Pergamon Press, 1960)
[7] I.E. Dzyaloshinskii. Sov.Phys. JETP, **10** (3), 628 (1960).
[8] D.N. Astrov. Sov. Phys JETP, **13** (4), 729 (1961).
[9] V.J. Folen, G.T. Rado, E.W. Stalder. Phys. Rev. Lett., **6**, 607 (1961). DOI: 10.1103/PhysRevLett.6.607
[10] C.-W. Nan, M.I. Bichurin, Sh. Dong, D. Viehland, G. Srinivasan. J. Appl. Phys., **103**, 031101 (2008). DOI: 10.1063/1.2836410
[11] A.P. Pyatakov, A.K. Zvezdin. Phys.Usp., **55** (6), 557 (2012). DOI: 10.3367/UFNr.0182.201206b.0593

[12] A.A. Bukharaev, A.K. Zvezdin, A.P. Pyatakov, Y.K. Fetisov. Phys. Usp., **61** (12), 1175 (2018). DOI: 10.3367/UFNe.2018.01.038279
[13] C. Tu, Z. Chu, B. Spetzler, P. Hayes, C.-Z. Dong, X.-F. Liang, H.-H. Chen, Y.-F. He, Y.-Y. Wei, I. Lisenkov, H. Lin, Y.-H. Lin, J. McCord, F. Faupel, E. Quandt, N.-X. Sun. Materials, **12**, 2259 (2019). DOI: 10.3390/ma12142259
[14] C.M. Leung, X. Zhuang, D. Friedrichs, J. Li, R.W. Erickson, V. Laletin, M. Popov, G. Srinivasan, D. Viehland. Appl. Phys. Lett., **111**, 122904 (2017). DOI: 10.1063/1.4996242
[15] C.M. Leung, X. Zhuang, J. Xu, J. Li, G. Srinivasan, D. Viehland. Appl. Phys. Lett., **110**, 112904 (2017). DOI: 10.1063/1.4978751
[16] J. Zhai, J. Gao, C. De Vreugd, J. Li, D. Viehland, A.V. Filippov, M.I. Bichurin, D.V. Drozdov, G.A. Semenov, S.X. Dong. Eur. Phys. J. B, **71**, 383 (2009). DOI: 10.1140/epjb/e2009-00318-9
[17] D. Filippov, Y. Liu, P. Zhou, B. Ge, J. Liu, J. Zhang, T. Zhang, G. Srinivasan. J. Compos. Sci., **5** (11), 287 (2021). DOI: 10.3390/jcs5110287
[18] D.A. Filippov, T.O. Firsova, V.M. Laletin, N.N. Poddubnaya. Tech. Phys. Lett., **43**(3), 313 (2017). DOI: 10.1134/S106378501703018X.
[19] V.M. Laletin, A.I. Stognii, N.N. Novitskii, N.N. Poddubnaya. Tech. Phys. Lett., **40** (11), 969 (2014). DOI: 10.1134/S1063785014110078
[20] V.M. Sreenivasulu, V.M. Petrov, L.Y. Fetisov, Y.K. Fetisov, G. Srinivasan. Phys. Rev. B, **86**, 214405 (2012). DOI: 10.1103/PhysRevB.86.214405
[21] V.M. Laletin, D.A. Filippov, S.E. Mozzharov, I.N. Manicheva. Tech. Phys. Lett., **44** (4), 281 (2018). DOI: 10.1134/S1063785018040065

Translated by Y.Deineka